Geophysical Research Letters

RESEARCH LETTER
10.1029/2024GL112665

How Does Pacific Decadal Oscillation Modulate Extreme Heavy Rainfall Frequency Over Far East Asia?

Haerin Park[1], Taeho Mun[1], Dong-Hyun Cha[1,2], Myong-In Lee[1], Minkyu Lee[3], Seung-Ki Min[4], Baek-Min Kim[5], and Seok-Woo Son[6]

[1]Department of Civil, Urban, Earth, and Environmental Engineering, Ulsan National Institute of Science and Technology, Ulsan, South Korea, [2]School of Urban and Environmental Engineering, Ulsan National Institute of Science & Technology (UNIST), Ulsan, South Korea, [3]Renewable Energy Big Data Laboratory, Korea Institute of Energy Research, Daejeon, South Korea, [4]Division of Environmental Science and Engineering, Pohang University of Science and Technology, Pohang, South Korea, [5]Division of Earth Environmental System Science Major of Environmental Atmospheric Sciences, Pukyong National University, Busan, South Korea, [6]School of Earth and Environmental Sciences, Seoul National University, Seoul, South Korea

Key Points:

- During Korea's summer, extreme heavy rainfall events show a negative correlation with the Pacific Decadal Oscillation (PDO)
- During the negative-PDO, localized extreme precipitation increases over Korea
- The different effects of PDO in negative and positive could be because of the increasing of sea surface temperature over 30°N

Supporting Information:

Supporting Information may be found in the online version of this article.

Correspondence to:

D.-H. Cha,
dhcha@unist.ac.kr

Citation:

Park, H., Mun, T., Cha, D.-H., Lee, M.-I., Lee, M., Min, S.-K., et al. (2025). How does Pacific Decadal Oscillation modulate extreme heavy rainfall frequency over Far East Asia? *Geophysical Research Letters*, *52*, e2024GL112665. https://doi.org/10.1029/2024GL112665

Received 23 SEP 2024
Accepted 23 JAN 2025

Abstract We investigated the relationship between heavy rainfall events (HREs) and the Pacific Decadal Oscillation (PDO) occurring in Korea over Far East Asia for 40 years (1981–2020). Using K-means clustering on the low-level jet, we identified four clusters (C1–C4), with C1 being characterized by weaker synoptic conditions. Out of the four clusters, C1 represented localized extreme HREs compared with the other clusters. Interestingly, only the HRE frequency of C1 was found to have a strong negative correlation with PDO. During the negative-PDO, sea surface temperature increased above 30°N, which decreased the meridional temperature gradient. This weakened the atmospheric circulation and created thermodynamic instability (i.e., weakened upper jet, increased low-level temperature, higher atmospheric water capacity), creating a favorable environment for HRE in C1. However, this negative-PDO environment provided somewhat unfavorable conditions for other clusters (C2–C4), so the PDO impact was insignificant.

Plain Language Summary We investigated the relationship between heavy rainfall events (HREs) and the Pacific Decadal Oscillation (PDO) that occurred in Korea over Far East Asia from 1981 to 2020. A high negative correlation with PDO was found for localized heavy precipitation with short duration and heavy precipitation intensity over Korea. The main reason for the different impacts of PDO-phases is related to the large-scale environment. During the negative-PDO-phase, warm sea surface temperature anomaly above the mid-latitudes allowed Korea to contain more water vapor, providing favorable conditions for HREs. In addition, during the negative-PDO-phase, temperature increases above 30°N weaken the temperature gradient around the South Pacific, creating favorable conditions for the formation of heavy rainfall characterized by localized, short-lived heavy rainfall events due to the creating thermodynamic conditions.

1. Introduction

Extreme weather and climate events significantly impact the natural environment and human society and are among the most serious societal challenges under climate change (Easterling et al., 2000). Extreme precipitation caused by heavy rainfall events (HREs) has received much attention as one of the most destructive natural disasters that severely damage human life and socioeconomic activities (Kim et al., 2021; Ning et al., 2021). Many previous studies have suggested that extreme precipitation is becoming more frequent and increasing due to climate change (Alexander et al., 2006; Donat et al., 2016). However, the patterns of change in extreme precipitation have varied across regions in recent decades. (e.g., increases (decreases) in extreme precipitation in western (north) China). A number of studies have suggested that different regional variations in extreme precipitation are affected by internal climate variability (e.g., El Niño–Southern Oscillation, ENSO; Pacific Decadal Oscillation, PDO, etc.) associated with large-scale climate modes at different timescales (Manton et al., 2001; Zhai et al., 2005).

Many studies have shown that the leading mode of the tropical interannual variability, known as ENSO (El Niño-Southern Oscillation), plays a crucial role in controlling the annual variability of rainfall in the East Asia (EA) region (Chang et al., 2000; Chen et al., 1992). During a positive ENSO phase, the Western North Pacific Subtropical High (WNPSH) expands, increasing moisture transport, which in turn triggers heavy rainfall in EA.

Conversely, during a negative ENSO phase, anomalous low-pressure systems in EA result in decreased rainfall in northern China. However, it has been reported that the relationship between ENSO and summer precipitation in EA has weakened since the late 1970s. The variability of rainfall in EA is influenced not only by variations originating in tropical regions but also by changes occurring in mid-latitude and high-latitude regions. For example, the PDO (Pacific Decadal Oscillation) refers to longer-term sea surface temperature (SST) variability in the North Pacific compared to ENSO and has transitioned from a negative phase to a positive phase since the late 1970s. This shift in the PDO is considered a key factor causing decadal variability in East Asian summer rainfall and changes in the relationship with ENSO through teleconnections occurring in tropical and mid-high latitude regions. Recently, Song and Zhou (2015) found that the PDO influences the relationship between East Asian summer rainfall and ENSO through WNPSH. Feng et al. (2014) also showed that the PDO can affect the decaying speed of El Niño, leading to abnormal summer rainfall in China depending on the PDO phase. They further discovered that the shift in the PDO phases alters the ENSO life cycle, resulting in different impacts of ENSO on East Asian summer rainfall depending on the PDO phase.

Meanwhile, it has been reported that the characteristics of summer rainfall in Korea have changed over the past few decades (Choi, 2015; Ha et al., 2005; Moon et al., 2015). Specifically, studies based on observational records have focused on decadal changes in rainfall variability in Korea. For example, Ho et al. (2003) investigated the changes in the rainy season in Korea since the 1970s, while Kim et al. (2002) and Kwon et al. (2005) reported regime shifts in rainfall during the early 1980s and mid-1990s, respectively.

It is notable that there is considerable decadal variability in summer precipitation characteristics in EA, particularly in Korea. Nevertheless, our comprehension of the underlying mechanisms responsible for this decadal variability in Korea remains limited. Accordingly, this study aims to investigate the long-term variability of HREs that have caused extreme precipitation in Korea over the past 40 years (1981–2020). Subsequently, we examine the relationship between this long-term variability and long-term climate indices, such as the PDO, as well as the underlying physical mechanisms. Chapter 2 introduces the data and methods, Chapter 3 describes the results, and Chapter 4 provides a summary.

2. Data and Method

2.1. Data

Hourly precipitation data from the Korea Meteorological Administration (KMA) Automated Synoptic Observing System (ASOS) were used to identify HREs and analyze their precipitation characteristics (i.e., frequency, area, duration, and intensity). A total of 46 ASOS stations with continuous observations from 1981 to 2020 were considered. Meteorological variables from fifth-generation European Center for Medium-Range Weather Forecasts atmospheric reanalysis ERA5 data (Hersbach et al., 2020), with a 0.25° × 0.25° horizontal resolution and hourly (monthly) temporal resolution, were used to analyze the environmental features of HREs (PDO). The PDO index from the National Oceanic and Atmosphere Administration (http://psl.noaa.gov/gcos_wgsp/Timeseries/Data/pdo.long.data) was used to investigate the relationship between the summer PDO (June–September) and HREs in South Korea. The Niño 3.4 SST index was calculated using HadISST1, covering 5°S–5°N and 170–120°W (Rayner et al., 2003). The SST data set was taken from daily 0.25° Optimum Interpolation SST (OISST) version 2 (Reynolds et al., 2007).

2.2. Method

In this study, we defined an HRE according to the KMA heavy rainfall criteria as an event in which a single ASOS station recorded 6-hr rainfall accumulation exceeding 80-mm during the summer and early autumn months (from June to September) between 1981 and 2020. This definition aligns with KMA's HRE warning criteria. Even if an HRE was observed multiple times at various stations within a 6-hr period, we treated it as a single HRE. The reference time of each HRE was defined as the center of the 6-hr window of the accumulated rainfall, for example, 0600 UTC for 6-hr accumulated precipitation during 0300–0900 UTC. We excluded HREs caused by typhoons to analyze only local precipitation occurring during the rainy season or around Korea. Thus, a total of 505 HREs were selected for analysis, excluding events where tropical cyclones (TCs) with intensities above those of tropical storms (17 $m \cdot s^{-1}$) passed through the analysis area (27–47°N, 115–136°E). We obtained six-hourly TC data from the Joint Typhoon Warning Center for 40-year (1981–2020).

Although heavy rainfall in the analyzed area is influenced by various factors, one of its main driving factors in Korea is the lower-level jet (LLJ) (Hwang, 1993; Matsumoto, 1973). The LLJs transport warm moist air and produce convergence at their exit region to destabilize the environment (Higgins et al., 1997; Trier et al., 2006). In addition, LLJs can produce shear instability with strong wind shear (Mastrantonio et al., 1976; Sun & Zhai, 1980). Therefore, the K-means clustering algorithm (Hartigan & Wong, 1979) was applied using horizontal 700 hPa wind speed in the analysis area (27–47°N, 115–136°E) for each reference time of HREs with an hourly temporal resolution of ERA5 data. To validate the clustering analysis and determine the optimal number of clusters, we utilized the Krzanowski–Lai (KL) index (Krzanowski & Lai, 1988; Reynolds et al., 2007). This index helps ascertain the most suitable number of clusters by identifying where the KL-index is maximized, indicating the optimal clustering numbers. Our results indicated that dividing the wind speed into four clusters yielded the highest KL-index value (not shown), suggesting that four is the optimal number of clusters for this analysis.

3. Results

3.1. Recent Changes in Heavy Rainfall Characteristics

Based on the definition of HREs, 505 occurring in Korea were identified over 40-year (1981–2020). We employed K-means clustering analysis to characterize the synoptic features associated with HREs. Based on the results, the 505 HREs were divided into 146, 98, 175, and 86 events. Figure 1 shows the wind speed distribution at 700 hPa for each cluster (C1–C4), which exhibited distinct patterns. Compared with the other clusters, C1 exhibited a wind speed distribution with notably weaker intensity, primarily centered around the southern part of Korea (35°N, 130°E). C2 exhibited a relatively high wind speed, extending from the central region of the Korean Peninsula to the northeast. Conversely, C3 showed a band-shaped wind speed distribution extending northeast from the southeastern region of China across Korea. In C4, wind speed significantly strengthened to 20 $m \cdot s^{-1}$ and expanded from the lower reaches of the Yangtze River (30°N, 120°E) to Japan (35°N, 135°E). The distribution of wind speed influences the pattern and intensity of precipitation.

The HREs over South Korea are primarily driven by various atmospheric synoptic-scale processes (such as troughs, upper-level jets, and lower-level jets) that evolve over time. The related synoptic systems typically intensify as they move eastward over inland China and the Yellow Sea, eventually passing over South Korea and bringing heavy rainfall. Previous studies (Choi et al., 2008; Lee et al., 2008) have consistently linked heavy precipitation over Korea to the upper-level jet (ULJ). This is often accompanied by a southwesterly LLJ, which brings a substantial amount of moisture, and the entrance region of the ULJ induces upward motion on the equatorial side through thermally direct secondary circulation. This secondary circulation destabilizes the atmosphere, potentially facilitating the development of intense precipitation (Uccellini & Johnson, 1979; Uccellini & Kocin, 1987). In addition, strong vertical wind shear (VWS) in the lower atmosphere modulates dynamic instability, thereby controlling the intensity of convective systems and creating favorable conditions for convective development (Corbosiero & Molinari, 2002; Zhang & Atkinson, 1995).

In C2-C4, a strong trough forms and develops over inland China and the Yellow Sea 12–24 hr before precipitation occurs (Figures S1b–S1d in Supporting Information S1). As this trough moves eastward, synoptic conditions (i.e., upper(lower)-level winds, upward motion, moisture transport, and VWS intensify over Korea at the time of precipitation (Figure S2 in Supporting Information S1). These are HREs induced by dynamic factors associated with synoptic-scale systems formed in the west. In contrast, in C1, only very localized, small-scale lower-level dynamic instability conditions exist over Korea within 12 hr before precipitation occurs. However, the total column precipitable water (TCPW) distribution is high in all four clusters.

In conclusion, C2-C4 are mainly characterized by dynamically driven HREs associated with synoptic-scale systems that form and develop in the west (Figures S3b–S3d in Supporting Information S1), while C1 exhibits thermodynamic precipitation characteristics driven by high moisture content in the atmosphere and weak lower-level instability.

Figures 2a and 2b represent the probability density functions (PDFs) of the intensity and duration of precipitation, respectively. Precipitation intensity was defined as the 1-hr accumulated precipitation, while duration was the total time for which precipitation at the ASOS exceeded 5 $mm \cdot hr^{-1}$ (minimum 1-hr to maximum 6-hr). This analysis was only performed for ASOSs that exceeded 80 $mm \cdot 6\ hr^{-1}$ accumulated precipitation, which is the selection criterion for heavy rainfall. First, the PDF of the precipitation intensity showed that C1, C2, and C3 had

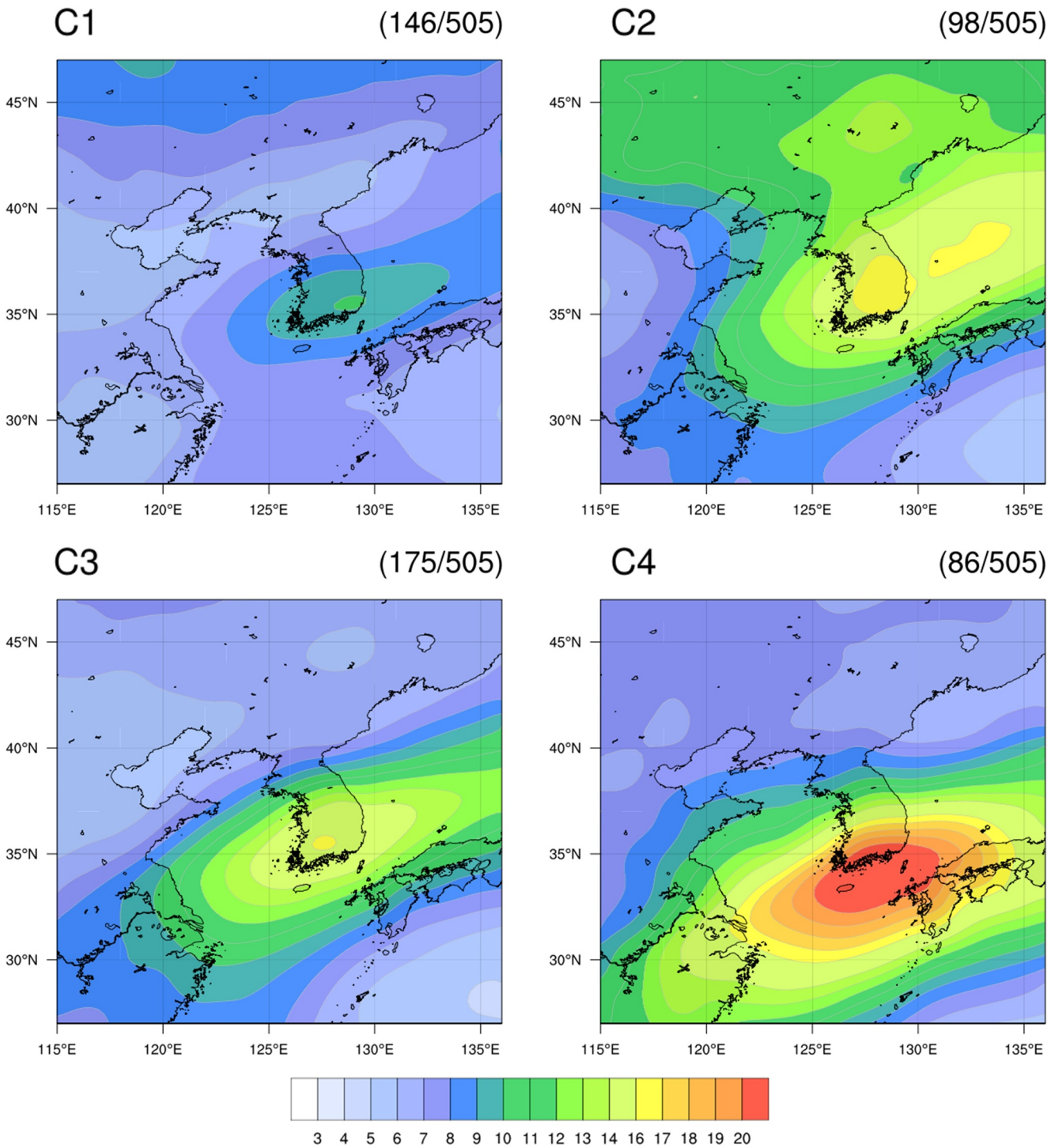

Figure 1. Composite 700 hPa wind speed patterns ($m \cdot s^{-1}$) for four HRE clusters.

similar characteristics, except for C4. When comparing C1, C2, and C3 with C4, there was a clear difference in the frequency of precipitation intensity between 10–20 and 40–120 $mm \cdot hr^{-1}$ (Figure 2a). C1, C2, and C3 were less frequent than C4 at precipitation intensities less than 30 $mm \cdot hr^{-1}$ and were more frequent at precipitation intensities exceeding 30 $mm \cdot hr^{-1}$ (Table S1 in Supporting Information S1). The duration also represented similar characteristics for C1, C2, and C3 except for C4 (Figure 2b). However, C1 predominantly showed a high frequency of events with short duration (less than 2-hr). As the duration increases (6-hr), the frequency in C1

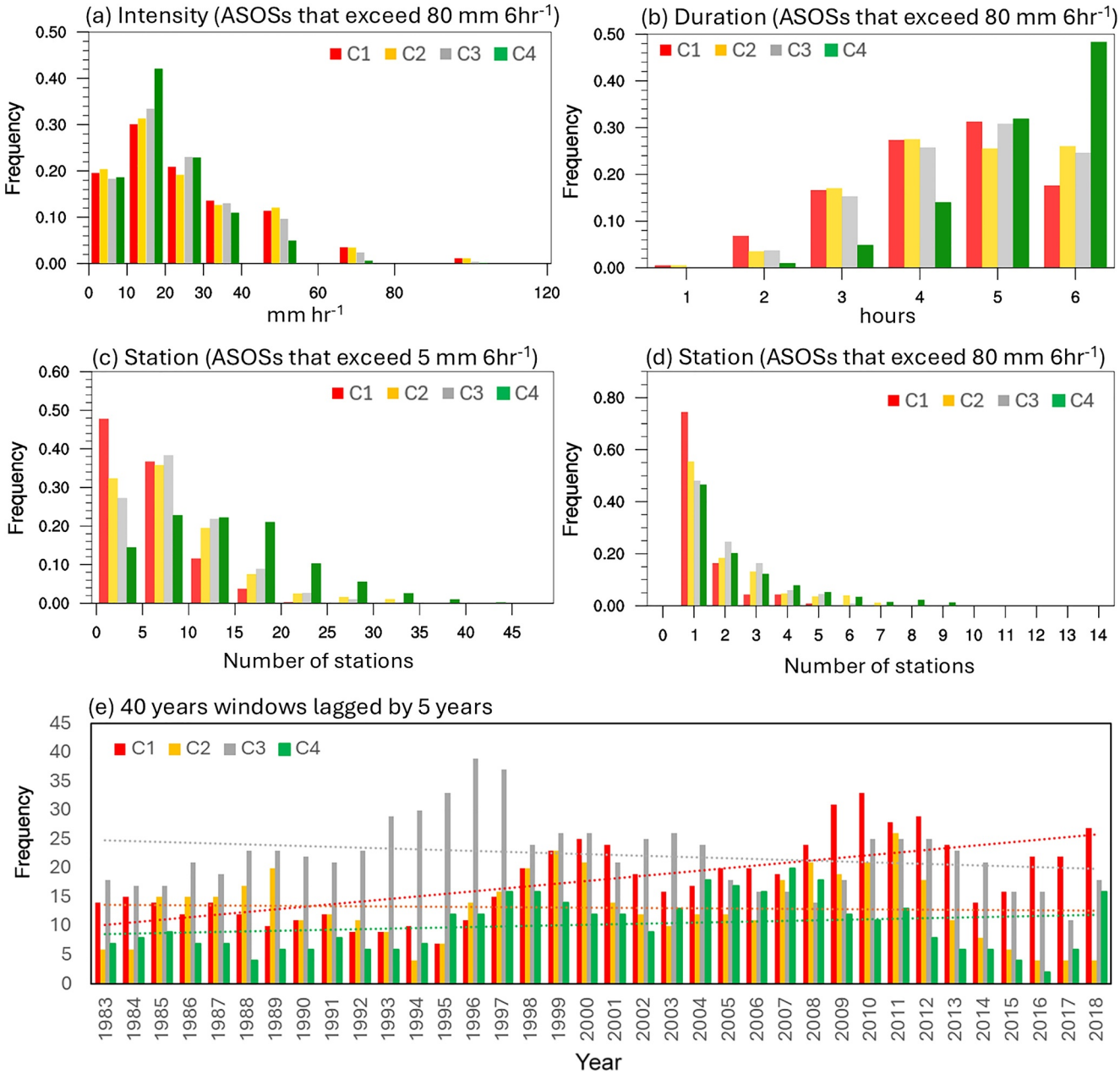

Figure 2. Probability density function (PDF) of (a) precipitation intensity (mm·hr^{-1}) and (b) precipitation occurrence time (duration) at ASOSs with intensities greater than 80 mm·6 hr^{-1}. PDF of the number of ASOS stations where the 6-hr accumulated precipitation was (c) >5 mm and (d) >80 mm during a single HRE. (e) Long-term variability and linear regression trend in HRE frequency (centered 5-year moving average) for each cluster.

markedly decreases. In contrast, C2 and C3 maintained a higher frequency at longer durations than C1. This indicated that C2 and C3 are likely to experience rainfall events that persist for relatively longer durations. C4, on the other hand, exhibited relatively low frequency in the short durations (1 ∼ 4-hr) but showed the highest frequency in the longest duration interval of 5 ∼ 6-hr. This pattern suggested that C4 was more likely to experience long-lasting rainfall events. Notably, C1 had the shortest precipitation duration among the four clusters.

The PDF of the number of ASOS stations with precipitation above a certain threshold was calculated to identify the precipitation areas for the HREs in each cluster (Figures 2c and 2d). Two thresholds were used: light (5 mm·6 hr^{-1}) and heavy precipitation (80 mm·6 hr^{-1}). Under light precipitation (Figure 2c), C1, C2, and C3 were concentrated at a small number of stations (10 or less), whereas C4 was concentrated at a moderate number of

stations (10–25). In other words, C1, C2 and C3 had fewer stations recording light precipitation (>5 mm·6 hr^{-1}) than C4. In particular, C1 exhibited smaller counts of stations recording light precipitation than C2 and C3, indicating that HREs in C1 typically resulted in the fewest stations recording precipitation intensities exceeding 5 mm·6 hr^{-1} compared with the other clusters. In contrast, the number of stations experiencing heavy precipitation was small in all clusters (Figure 2d). Among them, C1 had the fewest number of stations recording precipitation among all clusters, even during heavy precipitation exceeding 80 mm·6 hr^{-1}. In particular, for C1, about 80% of light precipitation (>5 mm) occurred at fewer than 10 stations, and for heavy precipitation (>80 mm), more than 80% occurred at fewer than two stations. Therefore, compared with the HREs in other clusters, the events in C1 indicated that precipitation was localized to a narrow region. These results suggest that the HREs in C1 represented extreme occurrences of concentrated heavy rainfall over a limited area within a short duration.

Figure 2e shows the long-term trends in the frequency of the annual mean HRE for each cluster. The Mann-Kendall test (Kendall, 1955; Mann, 1945) indicated that the long-term trend for C1 exhibited a statistically significant increase at the 99% confidence level. In contrast, the other clusters did not demonstrate any significant results. Therefore, analyzing the cause of the increasing trend in the HRE in C1 is important. Notably, C1 exhibited a period of interdecadal variability and tended to increase. This suggests that climatic factors are associated with the long-term variability of the HRE.

To identify the long-term variabilities related to HREs in Korea, we analyzed the correlation between the PDO index, Niño 3.4 index, and the annual HREs frequency. The climate index was calculated by averaging data from June to September, which is consistent with the period used for the precipitation frequency analysis. The correlations between the annual HRE frequency and climatic factors are shown in Table S2 in Supporting Information S1. For C2-C4, the correlation coefficients between the frequency and climate indices (PDO and Niño 3.4) indicated no significant relationship. However, in C1, there was a statistically significant correlation between the climate indices and frequency of HREs. In particular, this correlation showed a higher level of significance for the PDO than the Niño 3.4 index. It showed a negative correlation of −0.39 at the 90% confidence level, while the PDO exhibited a stronger negative correlation of −0.53 at the 99% confidence level. In addition, the partial correlation coefficient (Blair, 1918) between the HRE frequency and PDO was calculated to exclude the influence of ENSO. The partial correlation between the HRE frequency and PDO was −0.42 and was significant only in C1, while the other clusters (C2–C4) showed a weaker correlation with the HRE frequency and PDO (Figure S4 in Supporting Information S1). These results are similar to those presented in Table S2 in Supporting Information S1. Conversely, in C1, the partial correlation between the Niño 3.4 index and HRE was −0.18, excluding the influence of PDO. The result indicated that the PDO had the strongest influence on HRE frequency in C1, while the relationship in other clusters was comparatively weaker or not significant. Approximately 90% of the HRE of C1 occurred in July and August (not shown). Therefore, this study hereafter focuses on the relationship between the HRE frequency and PDO in C1 during these 2 months (July and August). The correlation between the HRE frequency of C1 and PDO during July and August was to be highly negative (−0.49) at the 99% confidence level (Figure 3; Table S2 in Supporting Information S1).

3.2. Comparison of HRE Frequency Between Positive- and Negative-PDO Years

In the previous section, we identified a significantly negative correlation between PDO and the HREs frequency for C1, which caused local extreme precipitation over a short period over the last 40 years. Hence, in this section, we analyze the effect of the PDO on HRE frequency by comparing the synoptic patterns for July and August in the negative- and positive-PDO years. Extreme PDO years were determined for the months when the PDO index was greater than 0.75 of a standard deviation. The years selected for the extreme PDO phases are listed in Table S3 in Supporting Information S1. To focus on the impact of the PDO, we excluded extreme PDO years that were also extreme ENSO years, which were defined by applying the same standard deviation criterion to the Niño 3.4 index as that applied for the extreme PDO years.

We analyzed potential causes for the difference between the two PDO phases in the HREs frequency for C1 by considering the monthly average anomalies field of SST, wind, ULJ, TCPW, VWS, and geopotential height (Figure 4). The SST patterns over the North Pacific during the negative- and positive-PDO-phases were almost opposite (Figures 4b and 4c). During the negative-PDO-phase, warm anomalies prevailed along 40°N from 120°E to 180°E, whereas cold anomalies were dominant in the positive-PDO-phase. These warm (cold) SST anomalies lead to atmospheric warming (cooling), which is more pronounced above 30°N, resulting in a smaller (larger)

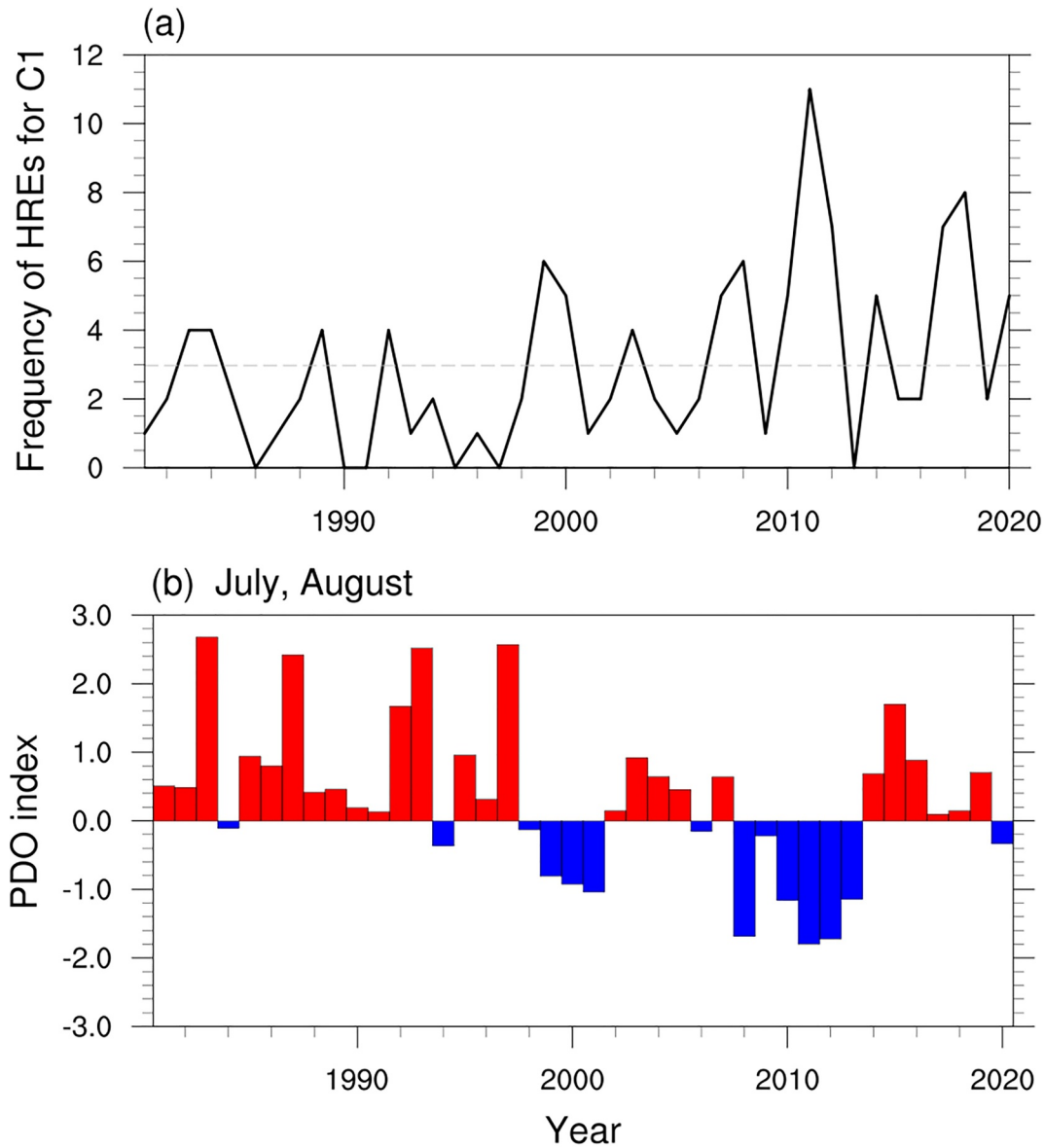

Figure 3. (a) Time series of HREs annual frequency for C1 (black solid line) and (5-year running mean frequency for C1 (red dashed line). (b) Time series of PDO index (bar) in July–August. The dashed line shows the mean of HREs frequency for C1 from July to August.

meridional temperature gradient during the negative (positive)-PDO-phase (Figure S5d in Supporting Information S1) (Lee et al., 2019; Park et al., 2015; Seo et al., 2015). Consequently, a smaller (larger) meridional temperature gradient during the negative (positive)-PDO-phase could result in a weak (strong) and easterly (westerly) anomalous ULJ due to the thermal–wind relationship (Lee et al., 2021; Yang et al., 2002). As a result, the negative-PDO-phase has a relatively weaker atmospheric circulation than the positive PDO phase.

Excessive TCPW in the atmosphere acts as one of the major causes of extreme precipitation events. Increasing atmospheric temperature can increase the water-holding capacity in the atmosphere, leading to changes in precipitation. An increase (decrease) of TCPW anomalies is clearly seen above 30°N during the negative (positive) PDO phase (Figures 4e and 4f). These TCPW anomalies closely correspond to SST anomalies. The correlation coefficient between the average TCPW for the Korea region (35–37.5°N, 125–130°E) and PDO was −0.55 at the 99% significance level. This indicates that the TCPW is significantly influenced by SST change in the PDO phase.

10.1029/2024GL112665

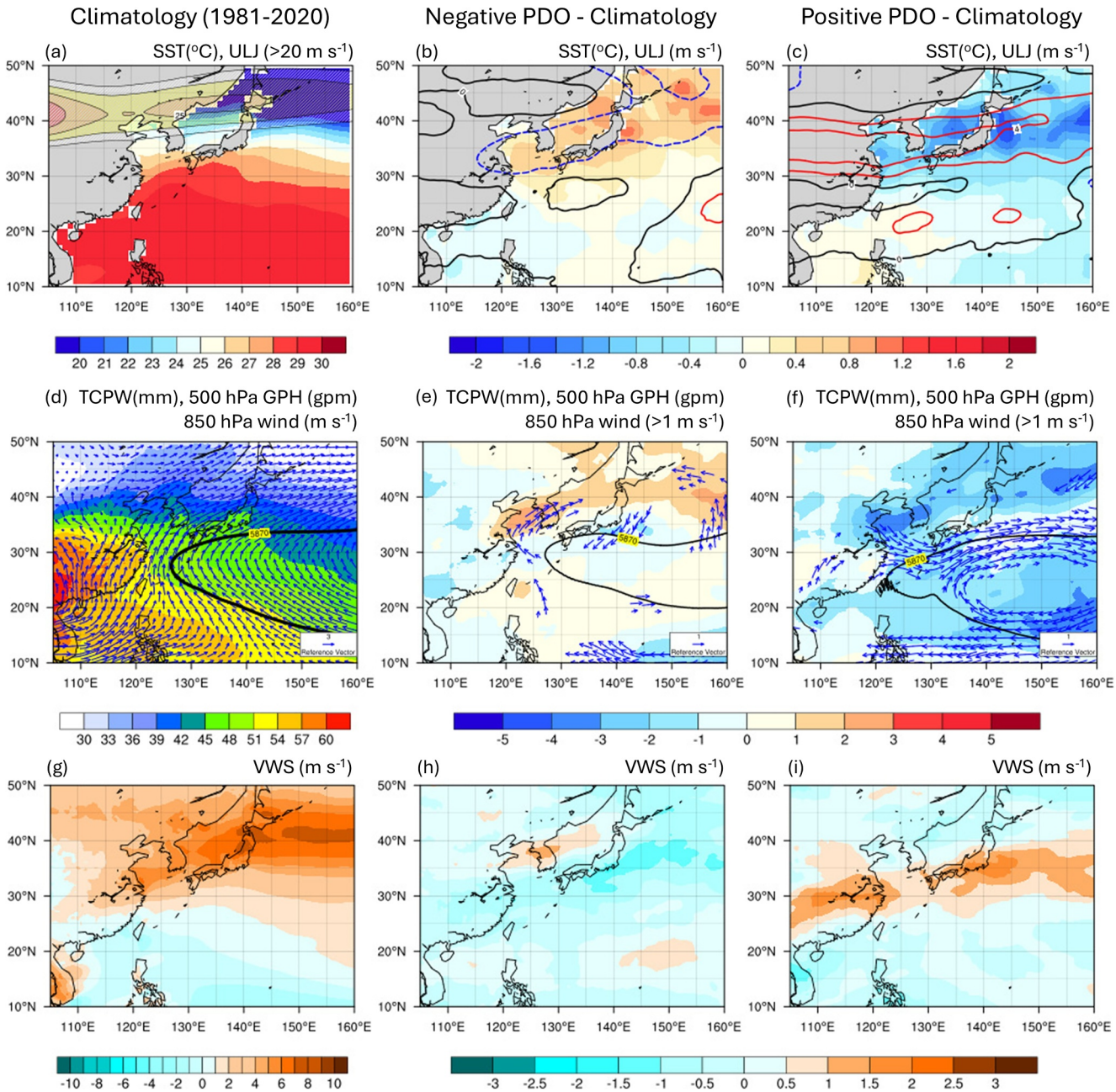

Figure 4. The spatial distribution of the (a–c) SST (shading, ºC), 200 hPa ULJ (contour, $m{\cdot}s^{-1}$), (d–f) 850 hPa wind (vector, $m{\cdot}s^{-1}$), 5870-gpm geopotential height (black contour), TCPW (shading, mm), and (g–i) zonal VWS (shading, U_{700hPa}-$U_{1000hPa}$, $m{\cdot}s^{-1}$). The left column (a, d, g) represents the climatology, calculated over the period of July-August from 1981 to 2020, using monthly ERA5 data. The middle (b, e, h) and right (c, f, i) columns show the anomalies for the negative- and positive-PDO-phases, respectively.

Additionally, there were differences in the position of the WNPSH between the two PDO phases. The WNPSH is a critical factor affecting heavy rainfall in the East Asian region, as it plays a role in controlling moisture transport and wind direction in the mid- and lower-levels of the atmosphere (Lee et al., 2013). The position of the WNPSH was identified based on the 5870-gpm geopotential height contour at 500 hPa (Cha & Lee, 2009; Yoon et al., 2018). During the negative-PDO-phase, the WNPSH was shifted northward and eastward compared to the climatological average, forming a positive lower-level wind anomaly over Korea. In contrast, during the positive-PDO-phase, the northern boundary of the WNPSH moves southward to 35°N, with a strong westerly wind anomaly forming along this boundary. Moreover, due to anomalous lower-level circulation, a weak positive zonal

VWS appears over Korea during the negative-PDO-phase, while a strong VWS is distributed along the 30°N during the positive-PDO-phase.

Why did the HREs frequency in C1 increase only during the negative-PDO-phase? As mentioned in Section 3.1, HREs in C1 were characterized by weak environmental conditions (e.g., the strength of upper and lower-level winds and integrated water vapor transport; see Figures S1 and S2 in Supporting Information S1) and were not significantly associated with strong synoptic-scale systems. Instead, they were driven by localized thermodynamic factors (e.g., TCPW, VWS). During the negative-PDO-phase, atmospheric circulation weakened, thermodynamic instability (e.g., increased atmospheric temperature and TCPW) was enhanced, and lower-level dynamic instability increased. These conditions created a favorable environment for the occurrence of HREs in C1. In contrast, the HREs of other clusters (C2-C4) are driven mainly by dynamical factors related to eastward propagating synoptic-scale systems, indicating that their occurrence is less influenced by the environmental changes associated with the PDO phase. Therefore, the negative-PDO-phase might have directly influenced the HREs frequency in C1 by creating thermodynamically favorable conditions for precipitation.

4. Summary and Conclusion

In this study, we conducted clustering analysis of 505 HREs (>80 mm·6 hr^{-1}) in Korea over 40-year (1981–2020) and analyzed the precipitation characteristics and long-term variability of heavy rainfall clusters. The identified HREs were categorized into four clusters using K-means clustering analysis based on the LLJ.

The HREs in C1 were characterized by weaker synoptic environments (i.e., ULJ, LLJ, and IVT) over Korea compared with the other clusters (C2–C4). However, the amount of TCPW was similar to that of other clusters. They also exhibited localized heavy rainfall features characterized by short-duration and high-intensity precipitation. Interestingly, a high negative correlation of −0.53 was found between the HREs frequency in C1 and PDO, such that the frequency significantly increased during the negative-PDO-phase. The difference in the large-scale environment was the main reason for the dissimilarity in the impacts of the two PDO phases. During the negative-PDO-phase, increasing temperatures above 30°N weakened the meridional temperature gradient around the mid-latitudes. This leads to a weakening atmospheric circulation and an increasing thermodynamic instability (i.e., increasing atmospheric temperature and TCPW, weakened ULJ), which was a favorable environment for HREs in C1. On the other hand, HREs in C2-C4 are mainly driven by strong eastward-propagating synoptic-scale systems (Figure S3 in Supporting Information S1) and are, therefore, not significantly affected by the PDO phase.

The results of this study provide a comprehensive understanding of the patterns, characteristics, and long-term variability in HREs in Korea, emphasizing the role of interdecadal climatic variability, particularly the PDO. We excluded the influence of extreme ENSO-years to better understand the relationship between PDO-phases and precipitation formation in Korea. In addition, this study focused on the characteristics of heavy rainfall in Korea. For future research, it is important to expand the investigation to other EA regions. Additionally, to enhance our understanding of the complex dynamics influencing HREs, a more detailed analysis of the combined effects of the PDO and ENSO is needed. Meanwhile, we also found that heavy rainfall is influenced by a combination of mid-latitude and high-latitude variability, and the HREs of C2 and C4 have positively correlated with the Atlantic Multidecadal Oscillation by 0.31 and 0.26, respectively. Therefore, additional research is needed to consider the possibility that HREs could be influenced by other atmospheric circulations. The limitations of the available precipitation data have constrained the analysis period in this study. An extension of the analysis period using a long-term data set is necessary to enhance the robustness of the findings.

The warming SST pattern in the WNP resembled that of the negative-PDO-phase. In recent decades, the SST in the mid-latitudes of the WNP has increased more significantly than that in other regions (Deser et al., 2010; Lee et al., 2019). Considering the pattern of the SST increase in the WNP, it would be valuable to study the similarities between warming and negative-PDO-phase conditions. Therefore, numerical model experiments (e.g., pseudo-global warming; Kawase et al., 2009; Lee et al., 2023) should be conducted to determine whether the changes in heavy precipitation in Korea are associated with natural variability or warming caused by human activity.

Recent changes in the characteristics of HREs over Korea, such as increases in small-scale and short-lived precipitation events, may indicate subtropicalization of precipitation characteristics. Small-scale precipitation events are difficult to predict (Park et al., 2024). Further research is therefore required to improve the

predictability of such precipitation by applying more advanced techniques, such as artificial intelligence (AI) and very-high-resolution modeling.

Data Availability Statement

Reanalysis file for ERA5 hourly data was downloaded from the National Center for Atmospheric Research's data archive via Hersbach et al. (2023). Figures have been made with the National Center for Atmospheric Research (NCAR) Command Language (NCL v6.6.1) post-processing tool accessible at https://www.ncl.ucar.edu [Software].

Acknowledgments
This work was supported by the Korea Meteorological Administration Research and Development Program under Grant RS-2024-00404042, and the National Research Foundation of Korea (NRF) grant funded by the Korea government (MSIT) (RS-2024-00350141).

References

Alexander, L. V., Zhang, X., Peterson, T. C., Caesar, J., Gleason, B., Klein Tank, A. M. G., et al. (2006). Global observed changes in daily climate extremes of temperature and precipitation. *Journal of Geophysical Research*, *111*(D5), D05109. https://doi.org/10.1029/2005jd006290

Blair, T. A. (1918). Partial correlation applied to Dakota data on weather and wheat yield. *Monthly Weather Review*, *46*(2), 71–73. https://doi.org/10.1175/1520-0493(1918)46<71:pcatdd>2.0.co;2

Cha, D. H., & Lee, D. K. (2009). Reduction of systematic errors in regional climate simulations of the summer monsoon over East Asia and the western North Pacific by applying the spectral nudging technique. *Journal of Geophysical Research*, *114*(D14), D14108. https://doi.org/10.1029/2008jd011176

Chang, C. P., Zhang, Y., & Li, T. (2000). Interannual and interdecadal variations of the East Asian summer monsoon and tropical Pacific SSTs. Part I: Roles of the subtropical ridge. *Journal of Climate*, *13*(24), 4310–4325. https://doi.org/10.1175/1520-0442(2000)013<4310:iaivot>2.0.co;2

Chen, L., Dong, M., & Shao, Y. (1992). The characteristics of interannual variations on the East Asian monsoon. *Journal of the Meteorological Society of Japan. Ser. II*, *70*(1B), 397–421. https://doi.org/10.2151/jmsj1965.70.1b_397

Choi, G. (2015). Spatio-temporal changes in seasonal multi-day cumulative extreme precipitation events in the Republic of Korea. *Journal of the Korean Association of Regional Geographers*, *21*(1), 98–113.

Choi, S. J., Cha, D. H., & Lee, D. K. (2008). Simulation of the 18-d summer heavy rainfall over East Asia using a regional climate model. *Journal of Geophysical Research: Atmospheres*, *113*(D12), D12101. https://doi.org/10.1029/2007jd009213

Corbosiero, K. L., & Molinari, J. (2002). The effects of vertical wind shear on the distribution of convection in tropical cyclones. *Monthly Weather Review*, *130*(8), 2110–2123. https://doi.org/10.1175/1520-0493(2002)130<2110:teovws>2.0.co;2

Deser, C., Phillips, A. S., & Alexander, M. A. (2010). Twentieth century tropical Sea surface temperature trends revisited. *Geophysical Research Letters*, *37*(10), L10701. https://doi.org/10.1029/2010gl043321

Donat, M. G., Lowry, A. L., Alexander, L. V., O'Gorman, P. A., & Maher, N. (2016). More extreme precipitation in the world's dry and wet regions. *Nature Climate Change*, *6*(5), 508–513. https://doi.org/10.1038/nclimate2941

Easterling, D. R., Meehl, G. A., Parmesan, C., Changnon, S. A., Karl, T. R., & Mearns, L. O. (2000). Climate extremes: Observations, modeling, and impacts. *Science*, *289*(5487), 2068–2074. https://doi.org/10.1126/science.289.5487.2068

Feng, J., Wang, L., & Chen, W. (2014). How does the East Asian summer monsoon behave in the decaying phase of El Niño during different PDO phases? *Journal of Climate*, *27*(7), 2682–2698. https://doi.org/10.1175/jcli-d-13-00015.1

Ha, K. J., Yun, K. S., Jhun, J. G., & Park, C. K. (2005). Definition of onset/retreat and intensity of Changma during the boreal summer monsoon season. *Korean Meteorological Society*, *41*(6), 927–942.

Hartigan, J. A., & Wong, M. A. (1979). Algorithm AS 136: A k-means clustering algorithm. *Journal of the Royal Statistical Society: Series A C*, *28*(1), 100–108. https://doi.org/10.2307/2346830

Hersbach, H., Bell, B., Berrisford, P., Biavati, G., Horányi, A., Muñoz Sabater, J., et al. (2023). ERA5 hourly data on single levels from 1940 to present. *Copernicus Climate Change Service (C3S) Climate Data Store (CDS)*. https://doi.org/10.24381/cds.adbb2d47

Hersbach, H., Bell, B., Berrisford, P., Hirahara, S., Horányi, A., Muñoz-Sabater, J., et al. (2020). The ERA5 global reanalysis. *Quarterly Journal of the Royal Meteorological Society*, *146*(730), 1999–2049. https://doi.org/10.1002/qj.3803

Higgins, R. W., Yao, Y., & Wang, X. L. (1997). Influence of the North American monsoon system on the US summer precipitation regime. *Journal of Climate*, *10*(10), 2600–2622. https://doi.org/10.1175/1520-0442(1997)010<2600:iotnam>2.0.co;2

Ho, C. H., Lee, J. Y., Ahn, M. H., & Lee, H. S. (2003). A sudden change in summer rainfall characteristics in Korea during the late 1970s. *International Journal of Climatology*, *23*(1), 117–128. https://doi.org/10.1002/joc.864

Hwang, L. (1993). A study on the relationship between heavy rainfalls and associated low-level jets in the Korean Peninsula. *Asia-Pacific Journal of Atmospheric Sciences*, *29*(2), 133–146.

Kawase, H., Yoshikane, T., Hara, M., Kimura, F., Yasunari, T., Ailikun, B., et al. (2009). Intermodel variability of future changes in the Baiu rainband estimated by the pseudo global warming downscaling method. *Journal of Geophysical Research*, *114*(D24), D24110. https://doi.org/10.1029/2009jd011803

Kendall, M. G. J. B. (1955). Further contributions to the theory of paired comparisons. *Biometrics*, *11*(1), 43–62. https://doi.org/10.2307/3001479

Kim, B. J., Kripalani, R. H., Oh, J. H., & Moon, S. E. (2002). Summer monsoon rainfall patterns over South Korea and associated circulation features. *Theoretical Applied Climatology*, *72*(1–2), 65–74. https://doi.org/10.1007/s007040200013

Kim, H., Lee, J. H., Park, H. J., & Heo, J. H. (2021). Assessment of temporal probability for rainfall-induced landslides based on nonstationary extreme value analysis. *Engineering Geology*, *294*, 106372. https://doi.org/10.1016/j.enggeo.2021.106372

Krzanowski, W. J., & Lai, Y. (1988). A criterion for determining the number of groups in a data set using sum-of-squares clustering. *Journal of Biometrics*, *44*(1), 23–34. https://doi.org/10.2307/2531893

Kwon, M., Jhun, J. G., Wang, B., An, S. I., & Kug, J. S. J. G. R. L. (2005). Decadal change in relationship between East Asian and WNP summer monsoons. *Geophysical Research Letters*, *32*(16), L16709. https://doi.org/10.1029/2005gl023026

Lee, D.-K., Cha, D.-H., Jin, C.-S., & Choi, S.-J. (2013). A regional climate change simulation over East Asia. *Asia-Pacific Journal of Atmospheric Sciences*, *49*(5), 655–664. https://doi.org/10.1007/s13143-013-0058-2

Lee, D.-K., Park, J.-G., & Kim, J.-W. (2008). Heavy rainfall events lasting 18 days from July 31 to August 17, 1998, over Korea. *Journal of the Meteorological Society of Japan. Ser. II*, *86*(2), 313–333. https://doi.org/10.2151/jmsj.86.313

Lee, M., Kim, T., Cha, D. H., Min, S. K., Park, D. S. R., Yeh, S. W., & Chan, J. C. (2021). How does Pacific Decadal Oscillation affect tropical cyclone activity over Far East Asia? *Geophysical Research Letters*, *48*(24), e2021GL096267. https://doi.org/10.1029/2021gl096267

Lee, M., Min, S.-K., & Cha, D.-H. (2023). Convection-permitting simulations reveal expanded rainfall extremes of tropical cyclones affecting South Korea due to anthropogenic warming. *npj Climate and Atmospheric Science*, *6*(1), 176. https://doi.org/10.1038/s41612-023-00509-w

Lee, S. H., Seo, K. H., & Kwon, M. (2019). Combined effects of El Niño and the Pacific Decadal Oscillation on summertime circulation over East Asia. *Asia-Pacific Journal of Atmospheric Sciences*, *55*(1), 91–99. https://doi.org/10.1007/s13143-018-00103-8

Mann, H. B. (1945). Nonparametric tests against trend. *Journal of the Econometric Society*, *13*(3), 245–259. https://doi.org/10.2307/1907187

Manton, M. J., Della-Marta, P. M., Haylock, M. R., Hennessy, K. J., Nicholls, N., Chambers, L. E., et al. (2001). Trends in extreme daily rainfall and temperature in Southeast Asia and the South Pacific: 1961–1998. *International Journal of Climatology*, *21*(3), 269–284. https://doi.org/10.1002/joc.610

Mastrantonio, G., Einaudi, F., Fua, D., & Lalas, D. P. (1976). Generation of gravity waves by jet streams in the atmosphere. *Journal of the Atmospheric Sciences*, *33*(9), 1730–1738. https://doi.org/10.1175/1520-0469(1976)033<1730:gogwbj>2.0.co;2

Matsumoto, S. (1973). Lower tropospheric wind speed and precipitation activity. *Journal of the Meteorological Society of Japan. Ser. II*, *51*(2), 101–107. https://doi.org/10.2151/jmsj1965.51.2_101

Moon, J. Y., Choi, Y., Kim, Y., & Kim, M. (2015). A study on the characteristics of summer extreme rainfall over South Korea in association with synoptic and large-scale circulation anomalies. *Journal of Climate Research*, *10*(4), 287–296. https://doi.org/10.14383/cri.2015.10.4.287

Ning, G., Luo, M., Zhang, Q., Wang, S., Liu, Z., Yang, Y., et al. (2021). Understanding the mechanisms of summer extreme precipitation events in Xinjiang of arid northwest China. *Journal of Geophysical Research: Atmospheres*, *126*(15). https://doi.org/10.1029/2020JD034111

Park, H., Hwang, J., Cha, D.-H., Lee, M.-I., Song, C.-K., Kim, J., et al. (2024). Does a scale-aware convective parameterization scheme improve the simulation of heavy rainfall events? *Journal of Geophysical Research: Atmospheres*, *129*(7), e2023JD039407. https://doi.org/10.1029/2023JD039407

Park, H.-l., Seo, K.-H., & Son, J.-H. (2015). Development of a dynamics-based statistical prediction model for the changma onset. *Journal of Climate*, *28*(17), 6647–6666. https://doi.org/10.1175/jcli-d-14-00502.1

Rayner, N. A. A., Parker, D. E., Horton, E. B., Folland, C. K., Alexander, L. V., Rowell, D. P., et al. (2003). Global analyses of sea surface temperature, sea ice, and night marine air temperature since the late nineteenth century. *Journal of Geophysical Research*, *108*, D14. https://doi.org/10.1029/2002jd002670

Reynolds, R. W., Smith, T. M., Liu, C., Chelton, D. B., Casey, K. S., & Schlax, M. G. (2007). Daily high-resolution-blended analyses for sea surface temperature. *Journal of Climate*, *20*(22), 5473–5496. https://doi.org/10.1175/2007jcli1824.1

Seo, K.-H., Son, J.-H., Lee, J.-Y., & Park, H.-S. (2015). Northern East Asian monsoon precipitation revealed by airmass variability and its prediction. *Journal of Climate*, *28*(15), 6221–6233. https://doi.org/10.1175/jcli-d-14-00526.1

Song, F., & Zhou, T. (2015). The crucial role of internal variability in modulating the decadal variation of the East Asian summer monsoon–ENSO relationship during the twentieth century. *Journal of Climate*, *28*(18), 7093–7107. https://doi.org/10.1175/jcli-d-14-00783.1

Sun, S. Q., & Zhai, G. Q. (1980). On the instability of the low level jet and its trigger function for the occurrence of heavy rain-storms. *Scientia Atmospherica Sinica*, *4*(4), 327–337.

Trier, S. B., Davis, C. A., Ahijevych, D. A., Weisman, M. L., & Bryan, G. H. (2006). Mechanisms supporting long-lived episodes of propagating nocturnal convection within a 7-day WRF model simulation. *Journal of the Atmospheric Sciences*, *63*(10), 2437–2461. https://doi.org/10.1175/jas3768.1

Uccellini, L. W., & Johnson, D. R. (1979). The coupling of upper and lower tropospheric jet streaks and implications for the development of severe convective storms. *Monthly Weather Review*, *107*(6), 682–703. https://doi.org/10.1175/1520-0493(1979)107<0682:tcoual>2.0.co;2

Uccellini, L. W., & Kocin, P. J. (1987). The interaction of jet streak circulations during heavy snow events along the east coast of the United States. *Weather Forecasting*, *2*(4), 289–308. https://doi.org/10.1175/1520-0434(1987)002<0289:tiojsc>2.0.co;2

Yang, S., Lau, K., & Kim, K. (2002). Variations of the East Asian jet stream and Asian–Pacific–American winter climate anomalies. *Journal of Climate*, *15*(3), 306–325. https://doi.org/10.1175/1520-0442(2002)015<0306:voteaj>2.0.co;2

Yoon, D., Cha, D. H., Lee, G., Park, C., Lee, M. I., & Min, K. H. (2018). Impacts of synoptic and local factors on heat wave events over southeastern region of Korea in 2015. *Journal of Geophysical Research: Atmospheres*, *123*(21), 12081–12096. https://doi.org/10.1029/2018jd029247

Zhai, P., Zhang, X., Wan, H., & Pan, X. (2005). Trends in total precipitation and frequency of daily precipitation extremes over China. *Journal of Climate*, *18*(7), 1096–1108. https://doi.org/10.1175/jcli-3318.1

Zhang, J. W., & Atkinson, B. W. (1995). Stability and wind shear effects on meso-scale cellular convection. *Boundary-Layer Meteorology*, *75*(3), 263–285. https://doi.org/10.1007/bf00712697